

## Al-Cu-Fe alloys in the solar system: Going inside a Khatyrka-like micrometeorite (KT01) from the Nubian Desert, Sudan

Chi MA<sup>1</sup>, Jinping HU <sup>1</sup>, Martin D. SUTTLE <sup>2</sup>, Yunbin GUAN<sup>1</sup>, Thomas G. SHARP<sup>3</sup>, Paul D. ASIMOW <sup>1</sup>, Paul J. STEINHARDT <sup>4</sup>, and Luca BINDI <sup>5\*</sup>

<sup>1</sup>Division of Geological and Planetary Sciences, California Institute of Technology, Pasadena, California, USA

<sup>2</sup>School of Physical Sciences, The Open University, Walton Hall, Milton Keynes, UK

<sup>3</sup>School of Earth and Space Exploration, Arizona State University, Tempe, Arizona, USA

<sup>4</sup>Department of Physics, Princeton University, Princeton, New Jersey, USA

<sup>5</sup>Dipartimento di Scienze della Terra, Università di Firenze, Florence, Italy

\*Correspondence

Luca Bindi, Dipartimento di Scienze della Terra, Università di Firenze, Via La Pira 4, Florence I-50121, Italy.

Email: [lucabindi@unifi.it](mailto:lucabindi@unifi.it)

(Received 05 June 2023; revision accepted 02 October 2023)

**Abstract**—A recently described micrometeorite from the Nubian desert (Sudan) contains an exotic Al-Cu-Fe assemblage closely resembling that observed in the Khatyrka chondrite (Suttle et al., 2019; *Science Reports* 9:12426). We here extend previous investigations of the geochemical, mineralogical, and petrographic characteristics of the Sudan spherule by measuring oxygen isotope ratios in the silicate components and by nano-scale transmission electron microscopy study of a focused ion beam foil that samples the contact between Al-Cu alloys and silicates. O-isotope work indicates an affinity to either OC or CR chondrites, while ruling out a CO or CM precursor. When combined with petrographic evidence we conclude that a CR chondrite parentage is the most likely origin for this micrometeorite. SEM and TEM studies reveal that the Al-Cu alloys mainly consist of Al metal, stolperite (CuAl), and khatyrkite (CuAl<sub>2</sub>) together with inclusions in stolperite of a new nanometric, still unknown Al-Cu phase with a likely nominal Cu<sub>3</sub>Al<sub>2</sub> stoichiometry. At the interface between the alloy assemblage and the surrounding silicate, there is a thin layer (200 nm) of almost pure MgAl<sub>2</sub>O<sub>4</sub> spinel along with well-defined and almost perfectly spherical metallic droplets, predominantly iron in composition. The study yields additional evidence that Al-Cu alloys, the likely precursors to quasicrystals in Khatyrka, occur naturally. Moreover, it implies the existence of multiple pathways leading to the association in reduced form of these two elements, one highly lithophile and the other strongly chalcophile.

### INTRODUCTION

Aluminum is a highly reactive, refractory lithophile element, while Cu is a low-reactivity, moderately volatile chalcophile element. Consequently, the union of Al-Cu as a metallic alloy is a highly unusual combination. Prior to 1985, Al-Cu alloys were known exclusively as synthetic materials created under controlled laboratory conditions. However, Razin et al. (1985) provided the first report of

natural Al-Cu alloys recovered as detrital grains dispersed in soils from eastern Russia. Ultimately, these fragments were found to be part of the disaggregated CV chondrite Khatyrka (Bindi & Steinhardt, 2014; MacPherson et al., 2013; Steinhardt & Bindi, 2012) and, therefore, extraterrestrial in origin. Microanalysis revealed the presence of exotic quasicrystals intergrown with the silicate minerals and Al-Cu alloys. This included icosahedral Al-Cu-Fe quasicrystals (Bindi et al., 2009,

2011) and decagonal Al-Ni-Fe quasicrystals (Bindi et al., 2015a, 2015b), representing the first natural occurrence of these quasiperiodic materials. This class of matter has properties intermediate between crystalline and amorphous materials, being characterized by atomic structures that are ordered but aperiodic and, therefore, lack translational symmetry while retaining higher order symmetries (Levine & Steinhardt, 1984; Shechtman et al., 1984).

As the only natural example of Al-Cu alloys and quasicrystals, the Khatyrka meteorite has received significant research attention (Andronicos et al., 2018; Bindi et al., 2012; Lin et al., 2017; Ma et al., 2017; MacPherson et al., 2013; Meier et al., 2018; Tommasini et al., 2021; Wieler, 2023). This led to the hypothesis and experimental testing of a hypervelocity impact-induced origin for the Al-Cu alloys and their quasicrystal components (Asimow et al., 2016; Hollister et al., 2014; Hu et al., 2020; Oppenheim et al., 2017a, 2017b). However, skepticism regarding their authenticity persisted (Ivanova et al., 2017), primarily due to the exceptional nature of this find.

More recently, a second independent discovery of Al-Cu alloys was identified within a micrometeorite recovered from the Nubian desert, Sudan (Suttle et al., 2019). Although it does not contain quasicrystals, this particle (termed KT01) contains Al-Cu alloys and metallic Fe intermixed with silicate minerals, and therefore, exhibits close similarities to the Khatyrka meteorite. KT01 is a cosmic spherule and its parent body mineralogy was affected by flash heating during atmospheric entry (Genge et al., 2008).

The presence of at least three intermixed Fe-bearing Al-Cu alloy-bearing phases—aluminum, khatyrkite ( $\text{CuAl}_2$ ), and stolperite ( $\text{CuAl}$ )—whose textures and composition demonstrate rapid crystallization spanning at least from the  $\text{CuAl}_2 + \text{CuAl}$  peritectic ( $\sim 590^\circ\text{C}$ ; Zobac et al., 2019) to the  $\text{CuAl}_2 + \text{Al}$  eutectic ( $\sim 550^\circ\text{C}$ ) demonstrates that melting and quench cooling altered the pre-atmospheric mineralogy of the Al-Cu assemblage. The KT01 micrometeorite is otherwise a typical S-type cosmic spherule containing relict and neofomed olivine phenocrysts embedded within a mesostasis of Ca-bearing silicate glass. Particle textures preserve cumulate layering—indicative of rapid deceleration and high-orbital eccentricity prior to atmospheric entry (Suttle et al., 2019).

Despite detailed petrographic analysis, the crystallography of the Al-Cu alloys and the parent body provenance of KT01 remain poorly constrained. We set out to conduct a more detailed study of this particle. This study reports new data on the O-isotope composition of the silicate minerals in KT01 and a detailed transmission electron microscopy (TEM) investigation of the nano-scale mineralogy within the Al-Cu alloys and silicates in this sample.

## ANALYTICAL METHODS

The original mount containing the polished section of KT01 particle was made available for study by one of us (M.D.S.). Previously, as described in Suttle et al. (2019), the loose particle had been embedded in epoxy resin, sectioned, polished, and carbon coated before being studied under scanning electron microscope (SEM) by energy-dispersive X-ray (EDX) spectrometry, electron backscattered diffraction (EBSD) and wavelength dispersive spectrometry (WDS). Upon receipt of the sample, we conducted further research, as outlined.

Oxygen isotope measurements were performed at three locations deemed representative of the micrometeorite's silicate mineralogy; they sample primarily mesostasis material (Figure 1). These were acquired with a Cameca NanoSIMS 50L based at the Microanalysis Center, Division of Geological & Planetary Sciences, Caltech. A primary  $\text{Cs}^+$  beam of +8 keV and  $\sim 30$  pA was used to sputter the sample in a rastering mode ( $3 \times 3 \mu\text{m}$ ). Secondary ion signals of  $^{16}\text{O}^-$ ,  $^{17}\text{O}^-$ , and  $^{18}\text{O}^-$  were simultaneously collected with electron multipliers on the multicollection system, under high mass resolution conditions that resolve any interferences to the mass peaks of interest. Uncertainties on each data point include its counting statistical errors and the standard deviation of repeated measurements of the San Carlos olivine standard.

High-resolution scanning electron microscopy (SEM), energy-dispersive X-ray spectroscopy (EDS), and electron backscatter diffraction (EBSD) analyses were performed using a ZEISS 1550VP field emission SEM at the Division Analytical Facility of GPS, Caltech, to determine the composition and structure of the Al-Cu alloy phases and associated minerals in the KT01 section. Backscattered electron (BSE) imaging and quantitative EDS analyses (with an Oxford X-Max SDD system and an XPP correction procedure calibrated with Oxford factory internal standards) were carried out at 10 kV in order to reduce the excitation volume and increase spatial resolution. EBSD analyses used an HKL system with the SEM operating at 20 kV and 6 nA in focused-beam mode with a  $70^\circ$  tilted stage and variable pressure mode (25 Pa); the procedure is described in Ma and Rossman (2008, 2009). The EBSD system was calibrated using a single-crystal silicon standard.

A focused ion beam (FIB) foil of the alloy assemblage including the contact with its silicate host was extracted using a FEI Nova 600 Nanolab DualBeam FIB and SEM at the Kavli Nanoscience Institute of Caltech. The foil was milled with a 30 kV Ga ion beam to 500 nm thickness, placed on a Ted Pella molybdenum grid and further thinned to 100 nm with an 8 kV Ga ion beam.

Transmission electron microscopy analysis was performed on a FEI CM200-FEG in the Eyring Materials

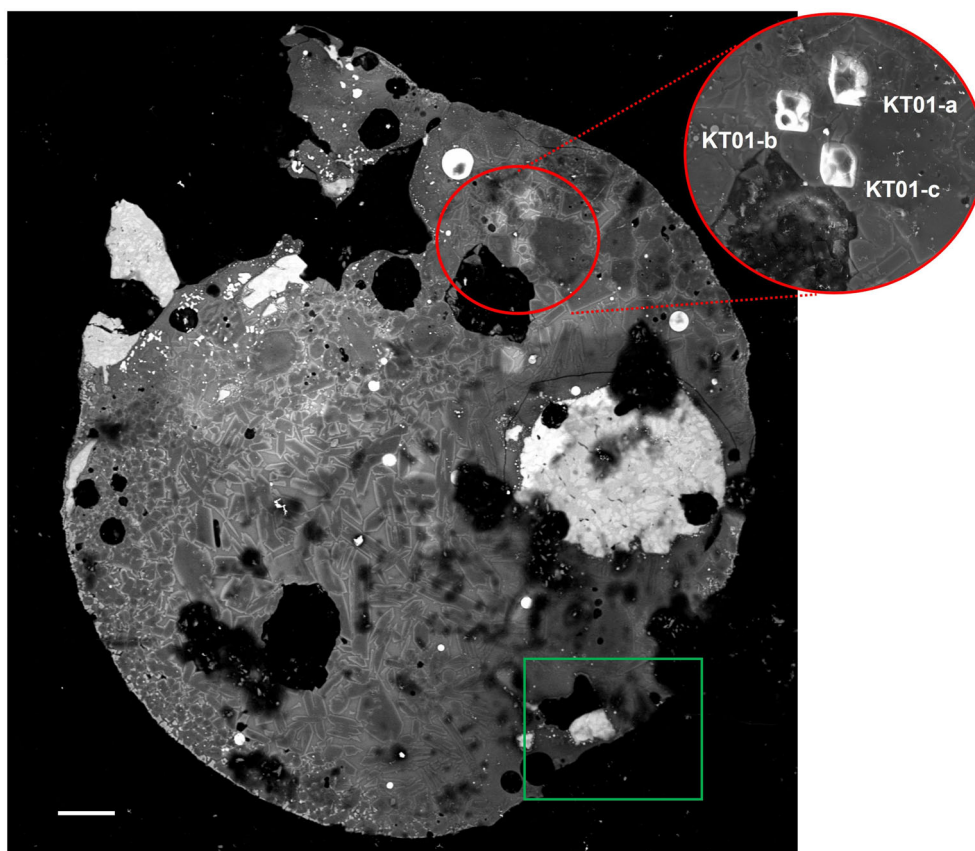


FIGURE 1. SEM-BSE image (left) of the KT01 micrometeorite with three pits generated by nanoSIMS measurements in the silicate mesostasis (red circle enlarged on the right in an SEM-BSE image to emphasize the topography). The green area is enlarged in Figure 2. The scale bar in the BSE image is 10  $\mu\text{m}$ . (Color figure can be viewed at [wileyonlinelibrary.com](http://wileyonlinelibrary.com).)

Center at Arizona State University. The TEM was operated at 200 kV. Bright field imaging and selected area electron diffraction (SAED) were used to characterize the texture and crystal structure of the alloy phases.

## RESULTS

### Oxygen Isotope Measurements

Three spot analyses returned data points ranging in  $\delta^{17}\text{O}$  from +2.1‰ to +2.8‰ ( $\pm 1.5\%$  [1 $\sigma$ ]), in  $\delta^{18}\text{O}$  from +3.7‰ to +5.9‰ ( $\pm 1.0\%$  [1 $\sigma$ ]), and in  $\Delta^{17}\text{O}$  from -0.7‰ to +0.9‰ ( $\pm 1.0\%$  [1 $\sigma$ ]). The average composition is  $\delta^{17}\text{O} = +2.4\%$ ,  $\delta^{18}\text{O} = +4.4\%$ , and  $\Delta^{17}\text{O} = +0.1\%$ , plotting within error on the terrestrial fractionation line (TFL; Figure 2).

### KT01 Metal Mineralogy

Contrast in SEM-BSE images demonstrates that the metallic assemblage in KT01 includes four different

phases (Figures 3 and 4). In order of increasing backscatter brightness (and hence increasing mean atomic number): Aluminum (*fcc*), khatyrkite ( $\theta$ , *I4/mcm*), stolperite ( $\beta$ , *Pm-3m*), and a new Al-Cu nanoinclusion (see next subsection for structural info). The Al phase is present in a eutectoid intergrowth with khatyrkite around some of the metallic regions (Figure 4c) but not those areas studied in detail here. Although phase domains  $\leq 1 \mu\text{m}$  in size are considered challenging for SEM analysis, a field emission instrument operated at low accelerating voltage can obtain quality single-phase EDS analyses using the  $K\alpha$  line of Al and the  $L\alpha$  line of Cu. EDS results (Table 1) show compositions closely resembling stolperite (CuAl) and khatyrkite (CuAl<sub>2</sub>) and are consistent with the previous electron microprobe data of the same micrometeorite sample (Ma et al., 2017; Suttle et al., 2019). The new Al-Cu phase is found as inclusions in stolperite up to 400 nm across. The composition of the largest domain (Figure 4a) matches best to a nominal Cu<sub>3</sub>Al<sub>2</sub> formula (Table 1), consistent with its BSE brightness clearly exceeding that of stolperite.

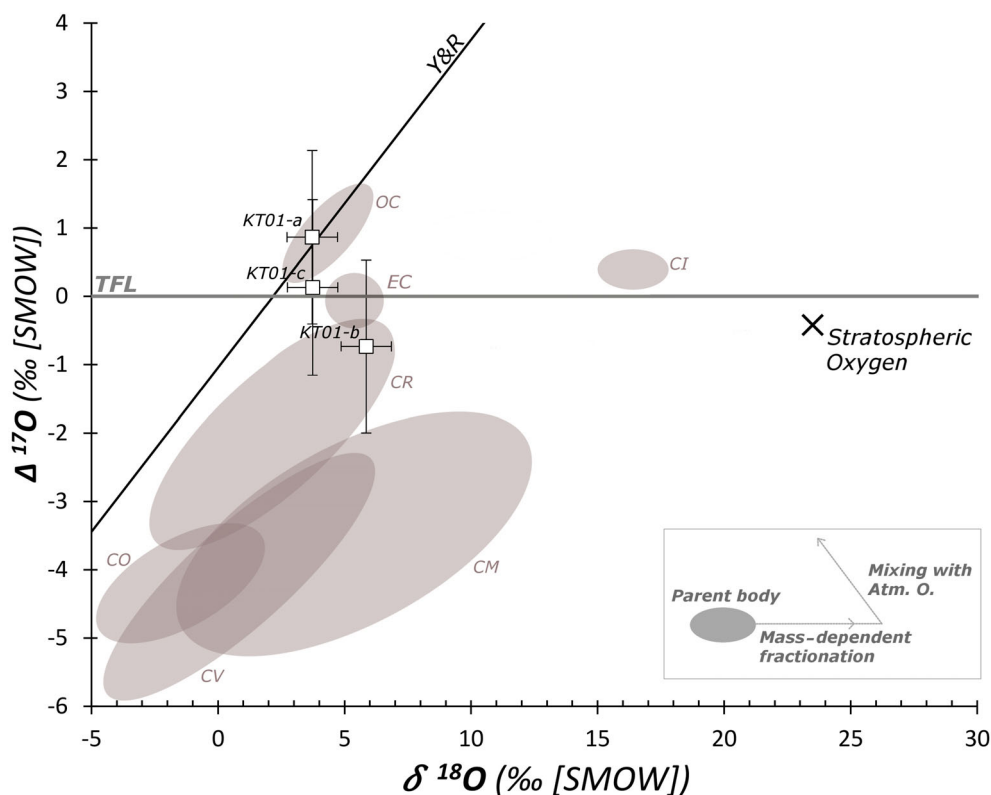


FIGURE 2. The O-isotope composition of KT01 (labeled squares with  $1\sigma$  uncertainties) is plotted in  $\delta^{18}\text{O}/\Delta^{17}\text{O}$  isotope space. During atmospheric entry the pre-atmospheric O-isotope composition of micrometeorites is progressively altered by mass-dependent evaporation and partial equilibration (mixing) with terrestrial oxygen. The composition of stratospheric oxygen, shown by the large black cross was defined in Thiemens et al. (1995). For reference we also show the compositions of relevant chondrite groups, labeled and shaded in gray. These include the OCs, the ECs, and several carbonaceous chondrite groups (CO, CR, CM, CV, and CI). Data defining these regions were taken from Clayton & Mayeda (1984), Clayton et al. (1991), Clayton and Mayeda (1999), Moriarty et al. (2009), Schrader et al. (2011), Schrader et al. (2014), Kimura et al. (2020). The solid gray line labeled “TFL” represents the terrestrial fractionation line ( $\delta^{17}\text{O} = 0.52 \times \delta^{18}\text{O}$ ) and the solid black line labeled “Y&R” represents the Young and Russell line (Young & Russell, 1998). (Color figure can be viewed at [wileyonlinelibrary.com](http://wileyonlinelibrary.com).)

## Crystal Structures

The EBSD results are consistent with the EDS results and unambiguously identify the stolperite ( $\beta$ ) and khatyrkite ( $\theta$ ) structures (Figure 5). TEM SAED patterns again confirm these structures and, moreover, reveal superstructures in stolperite as well as a topotactic relationship between coexisting stolperite and khatyrkite (Figures 6 and 7). The stolperite pattern includes diffraction from the common  $3\times$  superstructures on  $\langle 100 \rangle$  and  $\langle 011 \rangle$  directions (Figure 6b; Gui et al., 2001), whereas the diffraction on  $\langle 111 \rangle$  direction is more complex, likely indicating a non-periodic large-scale superlattice. Besides the pronounced  $\langle 111 \rangle * 3\times$  superstructure, the apparent  $d$ -spacings represent  $12\times$  and/or  $6\times$  superstructures even though they are not expected based on previous studies of the CsCl-type  $\beta$  phase (Gui et al., 2001) and some of

diffraction spots are missing (Figure 6b). The observed topotaxy of adjacent domains takes the form of SAED patterns with the  $\langle 012 \rangle$  zone of stolperite superimposed on the  $\langle 012 \rangle$  zone of khatyrkite, with stolperite  $(100) \parallel$  khatyrkite  $(200)$  and stolperite  $(021) \parallel$  khatyrkite  $(042)$ ; Figure 7d). Although the  $d$ -spacings of diffraction spots were calibrated against gold standard, given the limited precision of TEM electron diffraction, it is still difficult to refine the unit-cell parameter of stolperite to better than  $2.9 \pm 0.1 \text{ \AA}$ . Nonetheless, in the superposed SAED pattern it is clear that the  $(400)$  diffraction of khatyrkite occurs at slightly greater  $d$ -spacing than the  $(200)$  diffraction of stolperite, confirming the coexistence of two structures and their orientation relationship. The structure of the Al-Cu nanoinclusion is still to be fully determined, but current EBSD data suggest a W-type *bcc* structure for the phase (Figure 5c).

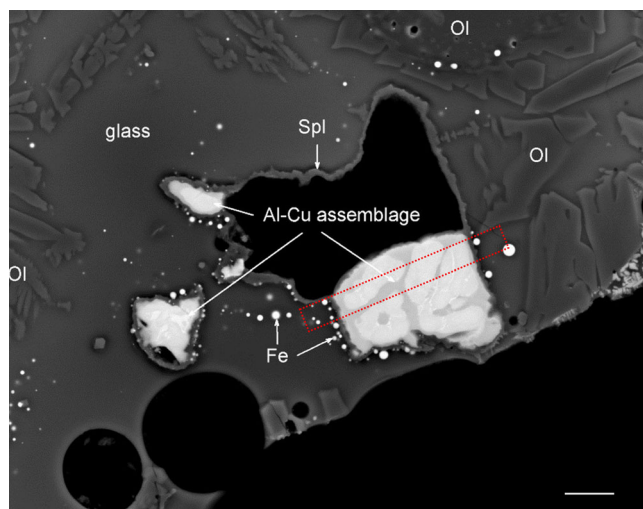


FIGURE 3. SEM-BSE image of the green area of Figure 1a showing the metallic Al-Cu assemblage. Ol—olivine, Spl—spinel, and Fe—iron. The shaded rectangle indicates the region where the FIB foil was sampled. (Color figure can be viewed at [wileyonlinelibrary.com](https://onlinelibrary.wiley.com/doi/10.1111/jmap.14089).)

### Textures of Silicate-Metallic Phases

On SEM-BSE images, khatyrkite domains appear homogeneous, whereas stolperite domains have resolvable brightness variations and white nanoinclusions (Figure 4). In contrast, in TEM bright field images, the khatyrkite domains commonly show a mottled texture along random zone axes, the result of a high density of defects (Figure 7b). The stolperite domains are more uniform under TEM imaging, although concentrated defects may show up in dark field images taken along specific reciprocal lattice vectors  $g$  (Figure 7c). The Al-Cu inclusions diffract more strongly than the surrounding stolperite (Figure 7a), consistent with a higher atomic weight (Table 1) and they commonly occur as elongated slabs in the FIB foil.

A thin layer (200 nm) of almost pure  $\text{MgAl}_2\text{O}_4$  spinel occurs at the interface between the alloy assemblage and the surrounding silicate. The silicate side of the spinel interface layer is also decorated by metallic droplets, predominantly iron in composition (Figures 3–7). The droplets are well-defined and almost perfectly circular in the FIB foil (and so presumably spherical in three dimensions).

## DISCUSSION

### Modification of the Al-Cu Alloys During Atmospheric Entry

The precursor of KT01 was extensively melted by heating during atmospheric entry; in this way it followed a very different thermodynamic path from the Khatyrka meteorite which, while recovered only as small detrital grains, was a larger mass at atmospheric entry and the bulk of it therefore experienced negligible heating. KT01 likely formed two immiscible liquids, one silicate and one metallic. These liquids reacted at their interface, as demonstrated by the presence of both Al and Cu within the quench-cooled silicate glass (Al: 8.7 wt%, Cu: 0.4 wt%) and the neoformed olivine phenocrysts (Al: 0.5 wt%, Cu: 0.2 wt%; Suttle et al., 2019). This exchange of components is presumed to have occurred during their short lifetime in the liquid phase before rapid cooling drove crystallization of each. The Fe droplets on the silicate side of the interface may represent Fe reduced from the silicate melt, coupled to oxidation of a share of the Al from the metal, leaving the metallic phase as a Cu-enriched nearly binary Cu-Al melt. In fact, except for the presence of <3 atom% of iron in the  $\text{CuAl}$  and  $\text{CuAl}_2$  phases (Table 1), we did not observe other characteristic Al-Cu-Fe phases in the low-Fe ternary system (Zhang et al., 2005; Zhang & Lück, 2003). Therefore, the Cu-Al phase equilibrium is more relevant (Suttle et al., 2019). At the interface, a layer of  $\text{MgAl}_2\text{O}_4$  grew from the two liquids, drawing on Al oxidized from the metal and MgO from the silicate. Upon crystallization, the silicate liquid crystallized zoned olivines and a fine or glassy metastasis. The metallic melt, whose bulk composition lies between  $\text{CuAl}_2$  and  $\text{CuAl}$ , would—according to available phase diagrams (Zobac et al., 2019)—begin by crystallizing a more copper-rich phase, likely the  $\epsilon'$  phase with  $\sim\text{Cu}_3\text{Al}_2$  composition and the NiAs structure, at around 800°C. The crystallization path would encounter a first peritectic reaction at 625°C,  $\text{Liquid} + \text{Cu}_3\text{Al}_2 \rightarrow \text{CuAl}$ , with the  $\text{CuAl}$  initially in a high-temperature structure ( $\eta$ , orthorhombic). This reaction would likely leave inclusions of  $\text{Cu}_3\text{Al}_2$  armored by  $\text{CuAl}$  material, preventing the consumption of the  $\text{Cu}_3\text{Al}_2$  by reaction with the liquid as it evolved toward Al-rich compositions. Upon further cooling to 590°C, the liquid would encounter another peritectic reaction,  $\text{Liquid} + \text{CuAl} \rightarrow$

FIGURE 4. (a, b) High-resolution BSE images of the metallic assemblages shown in Figure 3, including stolperite (Slp), khatyrkite (Ktk), and a new Cu-Al phase. Contrast has been optimized for viewing the various metal alloys; hence the silicate matrix appears black. The crystal size is generally in the range of 100–500 nm. The droplets in surrounding silicate glass are made of iron (Fe). The blue dots mark the regions for EDS analyses reported in Table 1. (c) BSE image showing a different metallic assemblage in KT01 with an Al + khatyrkite eutectoid intergrowth rim. (Color figure can be viewed at [wileyonlinelibrary.com](https://onlinelibrary.wiley.com/doi/10.1111/jmap.14089).)

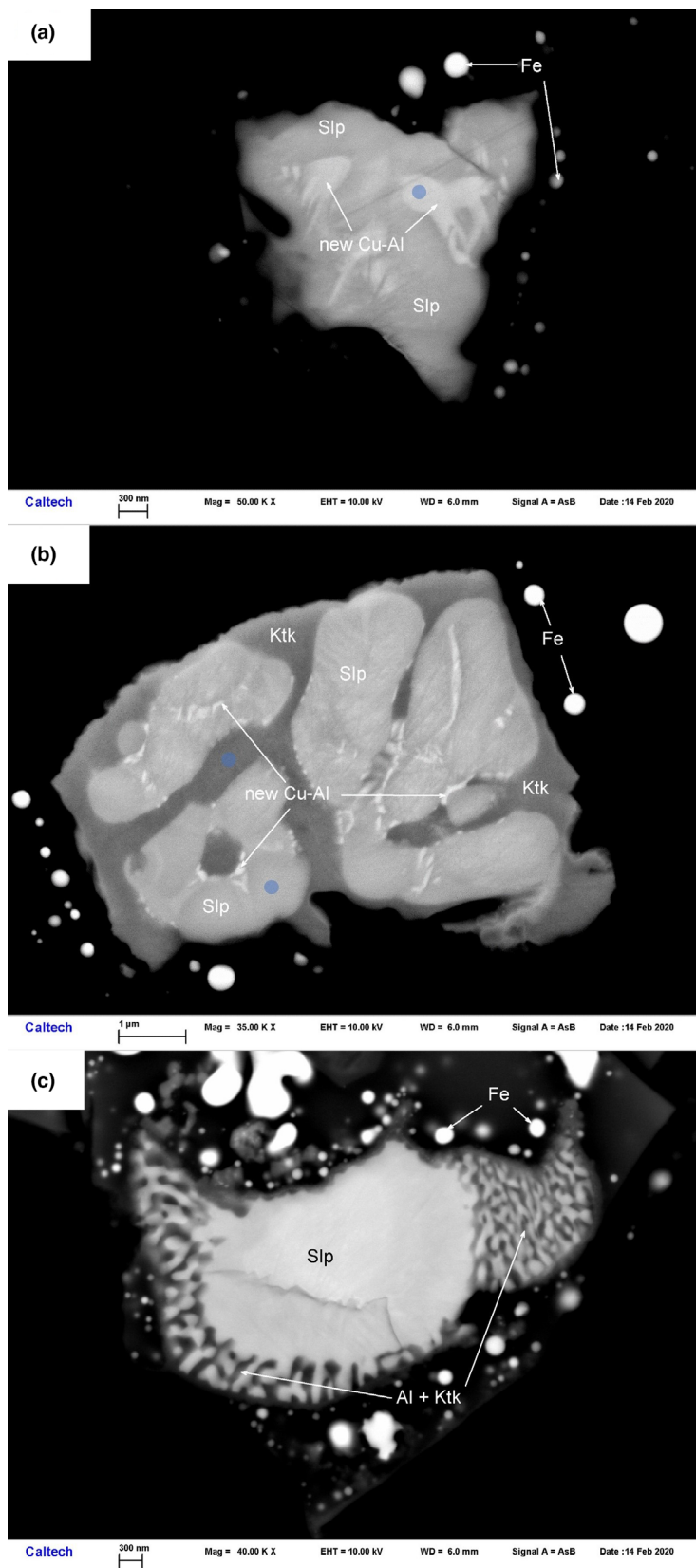


TABLE 1. Representative EDS chemical analyses of metallic phases.

	Al	Fe	Cu	Total
Cu-Al <sup>a</sup>	38.14	n.d.	61.86	100.00
Stolperite <sup>a</sup>	48.03	n.d.	51.97	100.00
Stolperite <sup>b</sup>	48.22	1.63	50.15	100.00
Stolperite <sup>c</sup>	47.95	2.60	49.45	100.00
Khatyrkite <sup>b</sup>	59.21	0.50	40.29	100.00

Note: Data in atomic percentage, normalized to 100%. Locations of the analyses are shown in Figure 4: <sup>a</sup>Figure 4a; <sup>b</sup>Figure 4b upper portion; <sup>c</sup>Figure 4b lower portion. Abbreviation: n.d., not detected.

CuAl<sub>2</sub>, which would consume more of the liquid and form khatyrkite domains surrounding and enveloping the CuAl domains. Meanwhile, also at about 590°C, the ε' phase of Cu<sub>3</sub>Al<sub>2</sub> would reach its lower stability limit and convert to another structure. The phase diagram does not show a W-type *bcc* phase in this region, but subsequent investigation of the structure of the Cu<sub>3</sub>Al<sub>2</sub> inclusions and consideration of kinetics of rapid cooling may resolve this issue. At 570°C, the high-temperature orthorhombic CuAl would invert to low-temperature monoclinic CuAl and ultimately transform to CsCl-type, because of the presence of trivial iron in the system (Table 1) (Zhang et al., 2005). Previous studies show that at the low-Fe end, the CsCl-type AlCu commonly shows <111>\*/3× superstructure around 600°C and <110>\*/10× superstructure around 500°C (referred to as the φ phases; Zhao et al., 2003). In our sample, we observed the coexistence of CsCl-type phases including stolperite (β) with no superstructure (Figure 7d); with pronounced 3× modulation superstructure on <100>, <110>, and <111>; and with complex quasi-12× modulation superstructure on <111>. Although the observed superstructures do not exactly match the experimental phase equilibrium predictions, the assemblage indicates the sample was quenched while undergoing a series of phase transitions. Finally, residual Al-rich liquid, isolated by peritectic rims from the Cu-rich phases, would eventually reach the khatyrkite + Al eutectic at 550°C and crystallize the fine intergrowth of these two phases observed at the boundaries of some metallic domains. This crystallization pathway explains the observed assemblage of Cu<sub>3</sub>Al<sub>2</sub> inclusions in stolperite, intermixed in turn with khatyrkite, and finally rimmed in some places by Al + khatyrkite.

### The Parent Body Affinity of the KT01 Micrometeorite

Oxygen isotopes can be used to link individual micrometeorites to established meteorite groups and thereby constrain their parent body provenance (Goderis et al., 2020; Rudraswami et al., 2022; Suavet et al., 2010; Suttle et al., 2020). However, before a direct comparison

between micrometeorite O-isotope data and bulk chondrite data can be made, three factors must be considered:

1. Chondritic meteorites are unequilibrated, heterogeneous assemblages containing high-temperature, <sup>16</sup>O-rich solid phases intermixed with lower temperature <sup>16</sup>O-poor phases (Clayton & Mayeda, 1984). Oxygen isotope measurements on small sample volumes typically reveal large intra-sample variation (e.g., Soens et al., 2020; Suttle et al., 2021). Thus, when analyzing micrometeorites their small size can result in an unrepresentative sampling of the parent body. For example, O-isotope data obtained from a micrometeorite may be strongly affected by sampling of a single mineral phase and not reflective of the bulk sample. As a result, isotopic data should always be considered alongside other diagnostic properties such as petrographic and geochemical data.
2. The O-isotope composition of cosmic spherules is systematically altered during atmospheric entry by two processes: evaporation and mixing. Evaporation induces a mass-dependent fractionation effect, forcing the micrometeorite's bulk O-isotope to evolve along a 0.52 slope in δ<sup>17</sup>O/δ<sup>18</sup>O isotope space, parallel to the TFL, and resulting in isotopically heavier compositions. Simultaneously, mixing between oxygen in the micrometeorite and atmospheric oxygen results in an evolution of the particle's bulk composition toward the composition of stratospheric oxygen (δ<sup>17</sup>O = +12.1‰, δ<sup>18</sup>O = +23.9‰, and Δ<sup>17</sup>O = −0.32‰; Pack et al., 2017; Thiemens et al., 1995). Notably, mixing and evaporative fractionation are most effective once particles melt and form cosmic spherules (as in the case of KT01).
3. NanoSIMS measurements of small sample volumes provide benefits of high spatial resolution but with the drawback of lower precision (relative to more traditional SIMS instruments analyzing significantly larger volumes). The data collected here have 1σ uncertainties between 1.0‰ and 1.5‰.

These factors (unrepresentative sampling, O-isotope evolution during atmospheric entry and large analytical uncertainties), make reconstructing the parent body affinity of KT01 uncertain. The combined sample heterogeneity and uncertainties of the three datapoints produce an area which straddles the TFL and overlaps the bulk compositional range of the ordinary chondrites (OCs), the enstatite chondrites (ECs) and the CR chondrites, suggesting that the parent body provenance of KT01 is most likely related to one of these groups.

An affinity to the ECs is unlikely based on the presence of abundant, small relict Mg-rich olivine grains (Fo82–89, Suttle et al., 2019; Table 1) in KT01. In contrast, olivine is both rare in ECs (<4.5 vol%) and

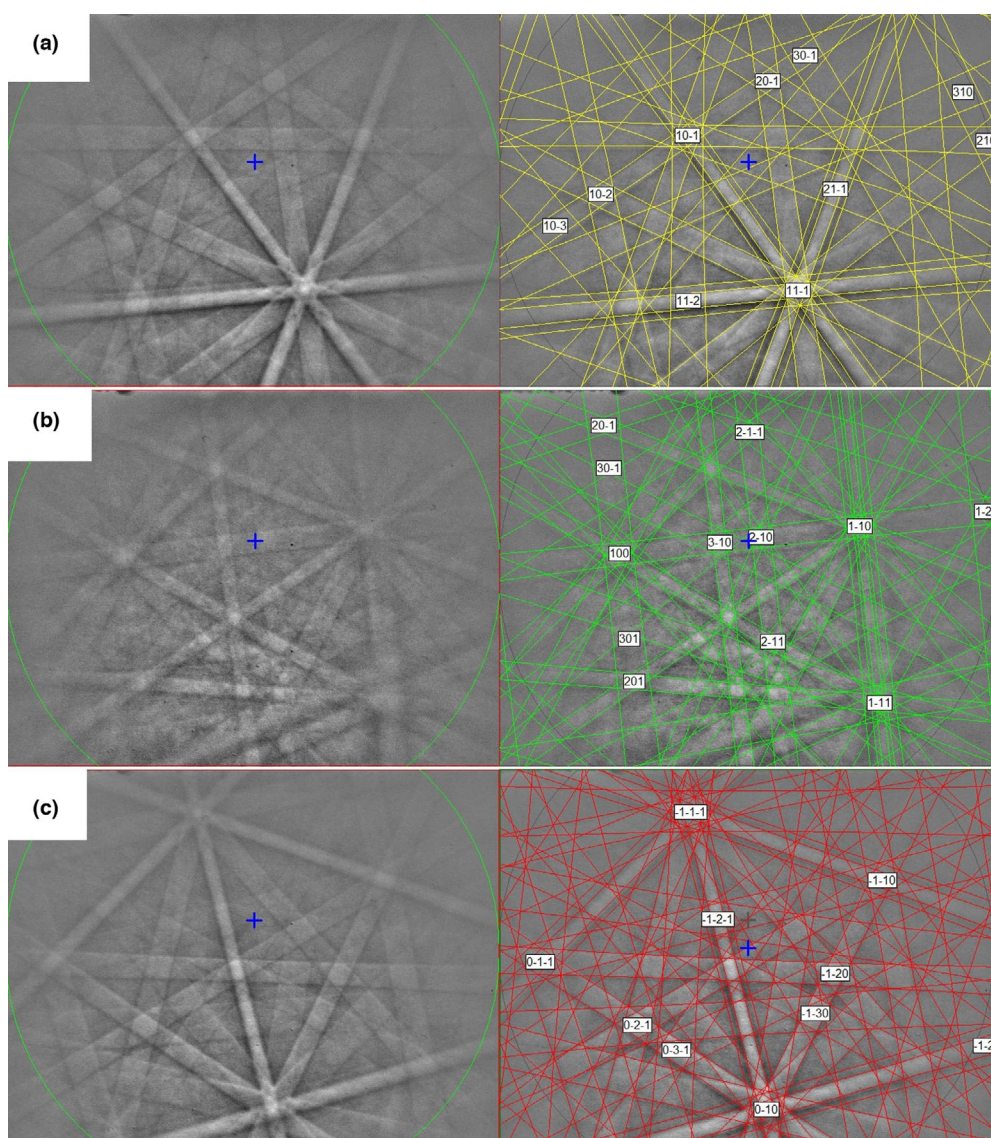


FIGURE 5. EBSD patterns (left column) with indexed structure solutions (right column) showing stolperite (a;  $Pm-3m$ ), khatyrkite (b;  $I4/mcm$ ), and the new Cu-Al phase (c). The new phase is indexed best with the W-type  $bcc$  structure. The blue cross indicates the center-point of the pattern. (Color figure can be viewed at [wileyonlinelibrary.com](http://wileyonlinelibrary.com).)

occurs almost exclusively as the forsterite endmember ( $Fo > 98$ ; Weisberg & Kimura, 2012). Additionally, the kamacite in KT01 contains minimal Si ( $\sim 0.1$  wt% in KT01) but Si is otherwise present at relatively high concentrations in EC metal ( $\sim 1.4$  wt%; Weisberg & Kimura, 2012).

Distinguishing between the other two parent body possibilities (OC vs. CR) requires further consideration of the micrometeorite's petrography. The absence of magnetite (except along the immediate particle perimeter), combined with the presence of droplets of near-pure Fe metal and the appearance of reduced relict olivine within the phenocryst cores demonstrates that the

entire melt, and not just the region proximal to the intermetallic alloy, experienced sustained reducing conditions. The pyrolysis of carbon is the most likely driver of reducing conditions in micrometeorites (Brownlee et al., 1997; Cordier & Folco, 2014; Genge & Grady, 1998; Taylor et al., 2005). To maintain these conditions during passage through an oxidizing atmosphere requires high abundances of carbon, which implies a carbonaceous chondrite, rather than an OC precursor. Furthermore, the  $\mu$ -porphyritic texture and presence of vesicles suggest that at least part of the micrometeorite was composed of hydrated material, which would be consistent carbonaceous chondrite

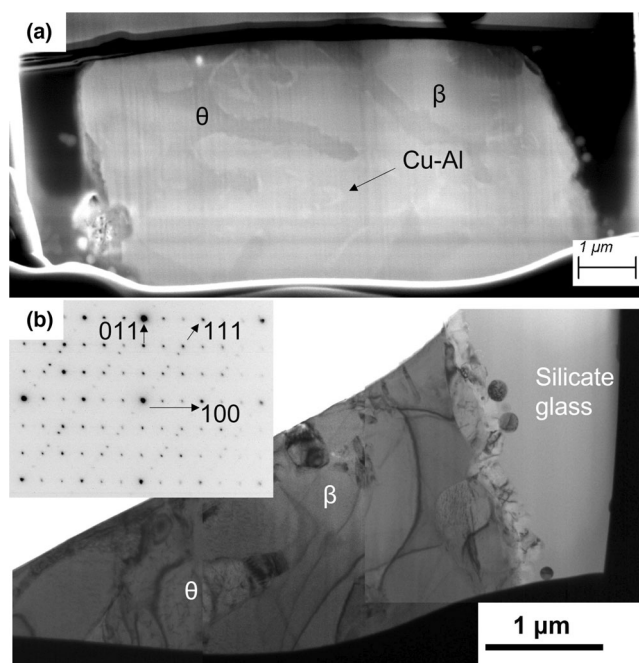


FIGURE 6. Images of a 100 nm FIB foil cut across a boundary between the metallic and silicate domains. (a) A BSE image of the FIB foil. The  $\theta$  (khatyrkite,  $I4/mcm$ ) and  $\beta$  (stolperite,  $Pm-3m$ ) phases are intergrown and the new Cu-Al phase occurs as nanoinclusions fully entrained in the  $\beta$  domains. (b) Mosaic of TEM bright field images showing elongated inclusions in  $\beta$  grains and the mottled textures from local defects in  $\theta$  grains. The metal/silicate interface shows a spinel layer and Fe droplets as in Figure 4. Inset is the diffraction pattern of  $\beta$   $\langle 011 \rangle$  zone, with  $3\times$  superstructure on  $\langle 100 \rangle^*$  and  $\langle 011 \rangle^*$  plus a complex superlattice on the 111 plane (see text). The  $d$ -spacing measured on the stolperite 100 diffraction is 2.84 Å.

matrix, as opposed to OC matrix (Van Ginneken et al., 2017). Additionally, the NiO contents of neoformed olivine microphenocrysts in cosmic spherules provide another mechanism of constrain the probable precursor material of micrometeorites, with Ni-poor (NiO  $<0.7$  wt%) compositions representing hydrated carbonaceous chondrites with high carbon contents (CM, CI, CR) and Ni-rich (NiO  $>0.7$  wt%) compositions representing carbon-poor, metal-rich bodies (CO, CV, CK, OC; Cordier et al., 2011). Wave dispersive EMPA data from the neoformed olivines were previously reported in Suttle et al. (2019; Table 1) and showed Ni-poor compositions (average NiO:  $0.28 \pm 0.14$  wt%,  $n = 7$ ) consistent with a CR, CM, or CI parent body.

The previous study of Suttle et al. (2019) argued that KT01 was derived from a carbonaceous chondrite precursor, and most likely a CO chondrite. Their conclusion was based on petrographic and geochemical evidence, namely the particle's  $\mu$ -porphyritic texture (Van Ginneken et al., 2017) and the minor element

composition of relict olivines (which overlaps the CM and CO compositional ranges). Although the new O-isotope data presented here rule out CO parentage (and the closely related CM chondrites), it leaves open the possibility of EC, OC, or CR chondrite source. Our re-evaluation of the petrographic data strongly suggests that KT01 derives from a carbonaceous chondrite parent body and, therefore, we conclude that a CR chondrite is the most likely precursor for this micrometeorite.

## CONCLUSIONS

Much of the controversy and mystery surrounding the discovery of quasicrystals in the Khatyrka meteorite centered on the fact that icosahedrite (Bindi et al., 2011),  $i$ -Phase II (Bindi et al., 2016), and several of the crystalline phases found closely associated with them (Ma et al., 2017; Razin et al., 1985) are alloys of aluminum (a high-temperature refractory lithophile) and copper (a low-temperature chalcophile). Native aluminum metal is an extremely rare occurrence, and up to that point, no other natural example of the co-occurrence of Al and Cu was known. Moreover, it was unclear how two metals with such different cosmochemistry could ever come together in any natural setting.

The discovery of KT01 proved that Al-Cu alloys are not unique to Khatyrka and not unique to the CV3 class of meteorites generally. Notwithstanding, the fact that the only two known examples of this type of material both originate from carbonaceous chondrite parent bodies seems to suggest that this material is unique to, or at least preferentially generated in, the outer solar system. However, in terms of explaining how Al-Cu alloys form naturally, the evidence presented in this paper only deepens the mystery because the evidence suggests a different pathway leading to the Al-Cu alloys in KT01 and in Khatyrka. In Khatyrka, impact-induced shock processing appears to have played an essential role in forming the alloys in general and the quasicrystals in particular, as shown by the presence of high-pressure phases and supported by laboratory shock experiments that reproduced them (e.g., Asimow et al., 2016). In KT01, we found no evidence of high-pressure phases, although the pronounced thermal processing experienced during atmospheric entry may have removed evidence of shock metamorphism. Also, KT01 is a cosmic spherule, while the Khatyrka grains originate from a larger “macroscopic” meteorite. In fact, its only similarity to Khatyrka, aside from the presence of Al-Cu alloys, is the presence of small Fe droplets at the silicate/metal interface and the rind of spinel, features consistent with the formation processes proposed by Lin et al. (2017) involving the “thermite” reaction coupling the reduction of FeO to the oxidation of metallic Al.

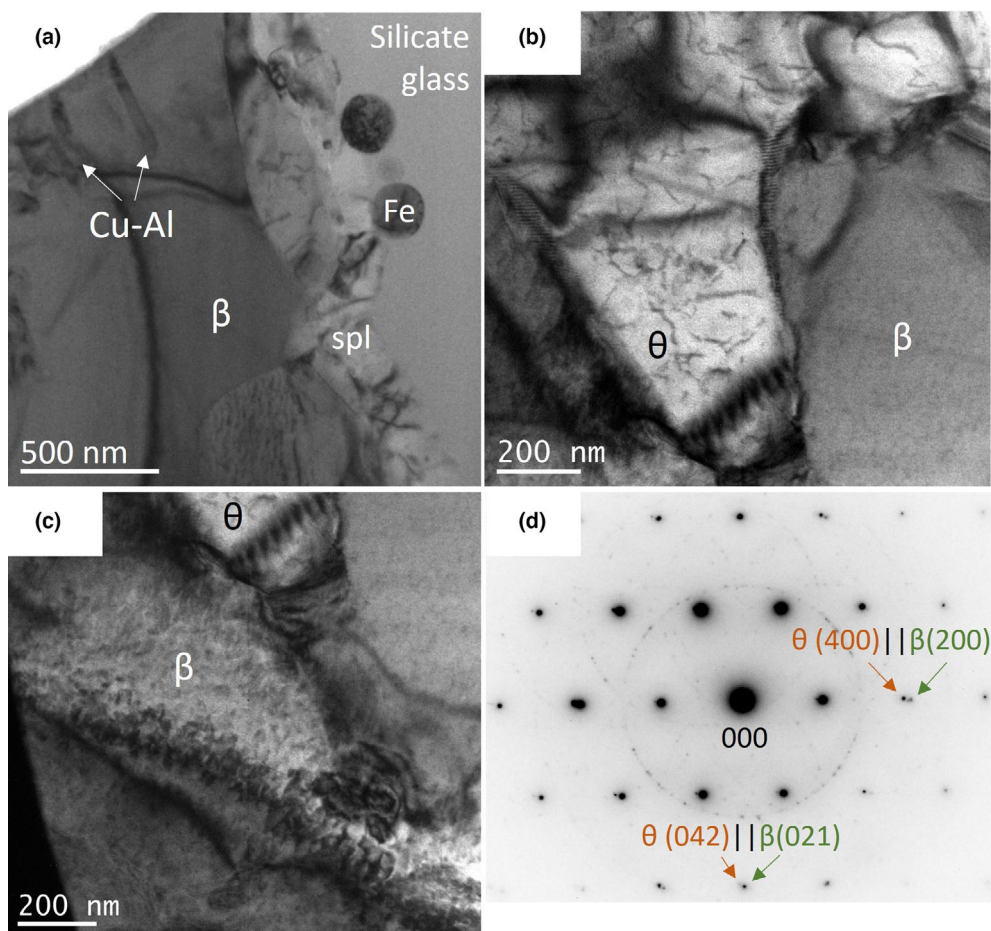


FIGURE 7. TEM images of the observed phases. (a) The alloy–silicate interface with spinel (spl) rim and Fe droplets (the same area is visible at lower magnification in Figure 6b). The Cu–Al nanophase is entrained in  $\beta$  (stolperite) domains. (b) The defect-rich texture in  $\theta$  (khatyrkite) contrasts with the smooth-looking  $\beta$  in bright field image. (c) Dark field image of  $\beta$  with  $g$  vector = 121 shows a moderate density of defects in stolperite. (d) SAED pattern indicates a superposition of the  $\theta$  and  $\beta$  patterns with a specific topotactic relationship involving parallel  $\langle 012 \rangle$  zones of both phases. Splitting of  $\theta$  (200) and  $\beta$  (400) reflections indicates that the (400)  $d$ -spacing of khatyrkite is slightly greater than the (200)  $d$ -spacing of stolperite. The  $d$ -spacing of the stolperite 100 diffraction is 2.97 Å. (Color figure can be viewed at [wileyonlinelibrary.com](http://wileyonlinelibrary.com).)

Understanding the unknown physical processes that led to these alloys is potentially important because they were probably present since the birth of the solar system and may have continued to occur through various mechanisms in later stages. Continued study of the existing specimens and attempts to reproduce them in the laboratory are leading to insights. Meanwhile, the search for more examples, though difficult, likely offers the most effective way to shed light on this mystery.

**Acknowledgments**—SEM, EBSD, and EDS analyses were carried out at the Caltech GPS Division Analytical Facility, which is supported, in part, by NSF Grants EAR-0318518 and DMR-0080065. TEM analyses were carried out in the Eyring Materials Center at Arizona State University, supported in part by NNCI-ECCS-1542160. The research was funded by MIUR-PRIN2017,

project “TEOREM deciphering geological processes using Terrestrial and Extraterrestrial ORE Minerals”, prot. 2017AK8C32 (PI: Luca Bindi).

**Conflict of Interest Statement**—The authors of this paper declare they have no conflict of interest.

**Data Availability Statement**—The data that support the findings of this study are available from the corresponding author upon reasonable request.

**Editorial Handling**—Dr. Donald E. Brownlee

## REFERENCES

- Andronicos, C., Bindi, L., Distler, V. V., Hollister, L. S., Lin, C., MacPherson, G. J., Steinhardt, P. J., and Yudovskaya,

- M. 2018. Comment on “Composition and Origin of Holotype Al-Cu-Zn Minerals in Relation to Quasicrystals in the Khatyrka meteorite” by M. Ivanova et al. (2017). *Meteoritics & Planetary Science* 53: 2430–40.
- Asimow, P. D., Lin, C., Bindi, L., Ma, C., Tschauer, O., Hollister, L. S., and Steinhardt, P. J. 2016. Shock Synthesis of Quasicrystals with Implications for their Origin in Asteroid Collisions. *Proceedings of the National Academy of Sciences of the United States of America* 113: 7077–81.
- Bindi, L., Eiler, J. M., Guan, Y., Hollister, L. S., MacPherson, G. J., Steinhardt, P. J., and Yao, N. 2012. Evidence for the Extra-Terrestrial Origin of a Natural Quasicrystal. *Proceedings of the National Academy of Sciences of the United States of America* 109: 1396–1401.
- Bindi, L., Lin, C., Ma, C., and Steinhardt, P. J. 2016. Collisions in Outer Space Produced an Icosahedral Phase in the Khatyrka Meteorite Never Observed Previously in the Laboratory. *Scientific Reports* 6: 38117.
- Bindi, L., and Steinhardt, P. J. 2014. The Quest for Forbidden Crystals. *Mineralogical Magazine* 78: 467–482.
- Bindi, L., Steinhardt, P. J., Yao, N., and Lu, P. J. 2009. Natural Quasicrystals. *Science* 324: 1306–9.
- Bindi, L., Steinhardt, P. J., Yao, N., and Lu, P. J. 2011. Icosahedrite,  $\text{Al}_{63}\text{Cu}_{24}\text{Fe}_{13}$ , the First Natural Quasicrystal. *American Mineralogist* 96: 928–931.
- Bindi, L., Yao, N., Lin, C., Hollister, L. S., Andronicos, C. L., Distler, V. V., Eddy, M. P., et al. 2015a. Natural Quasicrystal with Decagonal Symmetry. *Scientific Reports* 5: 9111.
- Bindi, L., Yao, N., Lin, C., Hollister, L. S., Andronicos, C. L., Distler, V. V., Eddy, M. P., et al. 2015b. Decagonite,  $\text{Al}_{71}\text{Ni}_{24}\text{Fe}_5$ , a Quasicrystal with Decagonal Symmetry from the Khatyrka CV3 Carbonaceous Chondrite. *American Mineralogist* 100: 2340–43.
- Brownlee, D. E., Bates, B., and Schramm, L. 1997. The Leonard Award Address Presented 1996 July 25, Berlin, Germany: The Elemental Composition of Stony Cosmic Spherules. *Meteoritics & Planetary Science* 32: 157–175.
- Clayton, R. N., and Mayeda, T. K. 1984. The Oxygen Isotope Record in Murchison and Other Carbonaceous Chondrites. *Earth and Planetary Science Letters* 67: 151–161.
- Clayton, R. N., and Mayeda, T. K. 1999. Oxygen Isotope Studies of Carbonaceous Chondrites. *Geochimica et Cosmochimica Acta* 63: 2089–2104.
- Clayton, R. N., Mayeda, T. K., Goswami, J. N., and Olsen, E. J. 1991. Oxygen Isotope Studies of Ordinary Chondrites. *Geochimica et Cosmochimica Acta* 55: 2317–37.
- Cordier, C., and Folco, L. 2014. Oxygen Isotopes in Cosmic Spherules and the Composition of the Near Earth Interplanetary Dust Complex. *Geochimica et Cosmochimica Acta* 146: 18–26.
- Cordier, C., van Ginneken, M., and Folco, L. 2011. Nickel Abundance in Stony Cosmic Spherules: Constraining Precursor Material and Formation Mechanisms. *Meteoritics & Planetary Science* 46: 1110–32.
- Genge, M. J., Engrand, C., Gounelle, M., and Taylor, S. 2008. The Classification of Micrometeorites. *Meteoritics & Planetary Science* 43: 497–515.
- Genge, M. J., and Grady, M. M. 1998. Melted Micrometeorites from Antarctic Ice with Evidence for the Separation of Immiscible Fe-Ni-S Liquids during Entry Heating. *Meteoritics & Planetary Science* 33: 425–434.
- Goderis, S., Soens, B., Huber, M. S., McKibbin, S., Van Ginneken, M., Van Maldeghem, F., Debaille, V., et al. 2020. Cosmic Spherules from Widerøefjellet, Sør Rondane Mountains (East Antarctica). *Geochimica et Cosmochimica Acta* 270: 112–143.
- Gui, J., Wang, J., Wang, R., Wang, D., Liu, J., and Chen, F. 2001. On some Discrepancies in the Literature about the Formation of Icosahedral Quasi-Crystal in Al-Cu-Fe Alloys. *Journal of Materials Research* 16: 1037–46.
- Hollister, L. S., Bindi, L., Yao, N., Poirier, G. R., Andronicos, C. L., MacPherson, G. J., Lin, C., et al. 2014. Impact-Induced Shock and the Formation of Natural Quasicrystals in the Early Solar System. *Nature Communications* 5: 4040.
- Hu, J., Asimow, P. D., Ma, C., and Bindi, L. 2020. First Synthesis of a Unique Icosahedral Phase from the Khatyrka Meteorite by Shock-Recovery Experiment. *IUCrJ* 7: 434–444.
- Ivanova, M. A., Lorenz, C. A., Borisovskiy, S. E., Burmistrov, A. A., Korost, D. V., Korochantsev, A. V., Logunova, M. N., Shornikov, S. I., and Petaev, M. I. 2017. Composition and Origin of Holotype Al-Cu-Zn Minerals in Relation to Quasicrystals in the Khatyrka Meteorite. *Meteoritics & Planetary Science* 52: 869–883.
- Kimura, M., Imae, N., Komatsu, M., Barrat, J. A., Greenwood, R. C., Yamaguchi, A., and Noguchi, T. 2020. The most Primitive CM Chondrites, Asuka 12085, 12169, and 12236, of Subtypes 3.0–2.8: Their Characteristic Features and Classification. *Polar Science* 26: 100565.
- Levine, D., and Steinhardt, P. J. 1984. Quasicrystals: A New Class of Ordered Structures. *Physical Review Letters* 53: 2477–80.
- Lin, C., Hollister, L. S., MacPherson, G. J., Bindi, L., Ma, C., Andronicos, C. L., and Steinhardt, P. J. 2017. Evidence of Redox Reaction in the Quasicrystal-Bearing Khatyrka Meteorite Reveals Multi-Stage Formation Process. *Scientific Reports* 7: 1637.
- Ma, C., Lin, C., Bindi, L., and Steinhardt, P. J. 2017. Hollisterite ( $\text{Al}_3\text{Fe}$ ), Kryachkoite ( $\text{Al,Cu}_6(\text{Fe,Cu})$ ), and Stolperite ( $\text{AlCu}$ ): Three New Minerals from the Khatyrka CV3 Carbonaceous Chondrite. *American Mineralogist* 102: 690–93.
- Ma, C., and Rossman, G. R. 2008. Barioperovskite,  $\text{BaTiO}_3$ , a New Mineral from the Benitoite Mine, California. *American Mineralogist* 93: 154–57.
- Ma, C., and Rossman, G. R. 2009. Tistarite,  $\text{Ti}_2\text{O}_3$ , a New Refractory Mineral from the Allende Meteorite. *American Mineralogist* 94: 841–44.
- MacPherson, G. J., Andronicos, C. L., Bindi, L., Distler, V. V., Eddy, M. P., Eiler, J., Guan, Y., et al. 2013. Khatyrka, a New CV3 Find from the Koryak Mountains, Eastern Russia. *Meteoritics & Planetary Science* 48: 1499–1514.
- Meier, M. M. M., Bindi, L., Heck, P. R., Neander, A. I., Spring, N. H., Riebe, M. E. I., Maden, C., et al. 2018. Cosmic History and a Candidate Parent Asteroid for the Quasicrystal-Bearing Meteorite Khatyrka. *Earth and Planetary Science Letters* 490: 122–131.
- Moriarty, G. M., Rumble, D., III, and Friedrich, J. M. 2009. Compositions of Four Unusual CM or CM-Related Antarctic Chondrites. *Geochemistry* 69: 161–68.
- Oppenheim, J., Ma, C., Hu, J., Bindi, L., Steinhardt, P. J., and Asimow, P. D. 2017a. Shock Synthesis of Five-Component Icosahedral Quasicrystals. *Scientific Reports* 7: 15629.
- Oppenheim, J., Ma, C., Hu, J., Bindi, L., Steinhardt, P. J., and Asimow, P. D. 2017b. Shock Synthesis of Decagonal Quasicrystals. *Scientific Reports* 7: 15628.

- Pack, A., Höweling, A., Hezel, D. C., Stefanak, M. T., Beck, A. K., Peters, S. T., Sengupta, S., Herwartz, D., and Folco, L. 2017. Tracing the Oxygen Isotope Composition of the Upper Earth's Atmosphere Using Cosmic Spherules. *Nature Communications* 8: 15702.
- Razin, L. V., Rudashevskij, N. S., and Vyalsov, L. N. 1985. New Natural Intermetallic Compounds of Aluminum, Copper and Zinc—Khatyrkite  $\text{CuAl}_2$ , Cupalite  $\text{CuAl}$  and Zinc Aluminides from Hyperbasites of Dunite-Harzburgite Formation. *Zapiski Vsesoyuznogo Mineralogicheskogo Obshchestva* 114: 90–100 (in Russian).
- Rudraswami, N. G., Suttle, M. D., Marrocchi, Y., Taylor, S., and Villeneuve, J. 2022. In-Situ O-Isotope Analysis of Relict Spinel and Forsterite in Small (<200  $\mu\text{m}$ ) Antarctic Micrometeorites—Samples of Chondrules & CAIs from Carbonaceous Chondrites. *Geochimica et Cosmochimica Acta* 325: 1–24.
- Schrader, D. L., Davidson, J., Greenwood, R. C., Franchi, I. A., and Gibson, J. M. 2014. A Water–Ice Rich Minor Body from the Early Solar System: The CR Chondrite Parent Asteroid. *Earth and Planetary Science Letters* 407: 48–60.
- Schrader, D. L., Franchi, I. A., Connolly, H. C., Jr., Greenwood, R. C., Lauretta, D. S., and Gibson, J. M. 2011. The Formation and Alteration of the Renazzo-Like Carbonaceous Chondrites I: Implications of Bulk-Oxygen Isotopic Composition. *Geochimica et Cosmochimica Acta* 75: 308–325.
- Shechtman, D., Blech, I., Gratias, D., and Cahn, J. W. 1984. Metallic Phase with Long-Range Orientational Order and no Translational Symmetry. *Physical Review Letters* 53: 1951–53.
- Soens, B., Suttle, M. D., Maeda, R., Vanhaecke, F., Yamaguchi, A., Van Ginneken, M., Debaille, V., Claeys, P., and Goderis, S. 2020. Evidence for the Presence of Chondrule-and CAI-Derived Material in an Isotopically Anomalous Antarctic Micrometeorite. *Meteoritics & Planetary Science* 55: 2703–26.
- Steinhardt, P. J., and Bindi, L. 2012. In Search of Natural Quasicrystals. *Reports on Progress in Physics* 75: 092601.
- Suavet, C., Alexandre, A., Franchi, I. A., Gattacceca, J., Sonzogni, C., Greenwood, R. C., Folco, L., and Rochette, P. 2010. Identification of the Parent Bodies of Micrometeorites with High-Precision Oxygen Isotope Ratios. *Earth and Planetary Science Letters* 293: 313–320.
- Suttle, M. D., Dionnet, Z., Franchi, I., Folco, L., Gibson, J., Greenwood, R. C., Rotundi, A., King, A., and Russell, S. S. 2020. Isotopic and Textural Analysis of Giant Unmelted Micrometeorites—Identification of New Material from Intensely Altered  $^{16}\text{O}$ -Poor Water-Rich Asteroids. *Earth and Planetary Science Letters* 546: 116444.
- Suttle, M. D., Folco, L., Genge, M. J., Franchi, I. A., Campanale, F., Mugnaioli, E., and Zhao, X. 2021. The Aqueous Alteration of GEMS-Like Amorphous Silicate in a Chondritic Micrometeorite by Antarctic Water. *Geochimica et Cosmochimica Acta* 293: 399–421.
- Suttle, M. D., Twegar, K., Nava, J., Spiess, R., Spratt, J., Campanale, F., and Folco, L. 2019. A Unique CO-Like Micrometeorite Hosting an Exotic Al-Cu-Fe-Bearing Assemblage—Close Affinities with the Khatyrka Meteorite. *Scientific Reports* 9: 1–9.
- Taylor, S., Delaney, J., Ma, P., Herzog, G. F., and Engrand, C. 2005. Isotopic Fractionation of Iron, Potassium, and Oxygen in Stony Cosmic Spherules: Implications for Heating Histories and Sources. *Geochimica et Cosmochimica Acta* 69: 2647–62.
- Thiemens, M. H., Jackson, T., Zipf, E. C., Erdman, P. W., and van Egmond, C. 1995. Carbon Dioxide and Oxygen Isotope Anomalies in the Meso- Sphere and Stratosphere. *Science* 270: 969–972.
- Tommasini, S., Bindi, L., Petrelli, M., Asimow, P. D., and Steinhardt, P. J. 2021. Trace Elements Conundrum of Natural Quasicrystals. *ACS Earth Space Chemistry* 5: 676–689.
- Van Ginneken, M., Gattacceca, J., Rochette, P., Sonzogni, C., Alexandre, A., Vidal, V., and Genge, M. J. 2017. The Parent Body Controls on Cosmic Spherule Texture: Evidence from the Oxygen Isotopic Compositions of Large Micrometeorites. *Geochimica et Cosmochimica Acta* 212: 196–210.
- Weisberg, M. K., and Kimura, M. 2012. The Unequilibrated Enstatite Chondrites. *Geochemistry* 72: 101–115.
- Wieler, R. 2023. A Journey in Noble Gas Cosmochemistry and Geochemistry. *Geochemical Perspectives* 12: 111–14.
- Young, E. D., and Russell, S. S. 1998. Oxygen Reservoirs in the Early Solar Nebula Inferred from an Allende CAI. *Science* 282: 452–55.
- Zhang, L., and Lück, R. 2003. Phase Diagram of the Al–Cu–Fe Quasicrystal-Forming Alloy System. *Zeitschrift für Metallkunde* 94: 91–97.
- Zhang, L., Schneider, J., and Lück, R. 2005. Phase Transformations and Phase Stability of the AlCuFe Alloys with Low-Fe Content. *Intermetallics* 13: 1195–1206.
- Zhao, D., Wang, R., Wang, J., Qu, W., Shen, N., and Gui, J. 2003. The Role of the  $\Phi$  Phase in the Solidification Process of Al–Cu–Fe Icosahedral Quasicrystal. *Materials Letters* 57: 4493–4500.
- Zobac, O., Kroupa, A., Zemanova, A., and Richter, K. W. 2019. Experimental Description of the Al-Cu Binary Phase Diagram. *Metallurgical and Materials Transactions A* 50: 3805–15.